Acta Pharmacologica Sinica

www.nature.com/aps

ARTICLE

Hepatocyte-derived VEGFA accelerates the progression of non-alcoholic fatty liver disease to hepatocellular carcinoma via activating hepatic stellate cells

Hao Shen[1], Han Yu[1], Qian-yu Li[2], Ya-ting Wei[1,3], Jing Fu[1], Hui Dong[1], Dan Cao[1], Lin-na Guo[1], Lei Chen[1], Yuan Yang[4], Ying Xu[1], Meng-chao Wu[1], Hong-yang Wang[1,3] and Yao Chen[1]

Non-alcoholic fatty liver disease (NAFLD) is emerging as an epidemic risk factor for hepatocellular carcinoma (HCC). The progression of NAFLD to HCC is closely associated with paracrine communication among hepatic cells. Vascular endothelial growth factor A (VEGFA) plays a key role in NAFLD and HCC; however, the cellular communication of VEGFA in the pathological transition from NAFLD to HCC remains unclear. Here, we found that VEGFA elevation was considerably distributed in hepatocytes of clinical and murine NAFLD-HCC specimens. Notably, progression from NAFLD to HCC was attenuated in hepatocyte-specific deletion of *Vegfa* (*Vegfa*$^{\Delta hep}$) mice. Mechanistically, VEGFA activated human hepatic stellate cell (HSC) LX2 into a fibrogenic phenotype via VEGF-VEGFR signaling in fatty acid medium, and HSC activation was largely attenuated in *Vegfa*$^{\Delta hep}$ mice during NAFLD-HCC progression. Additionally, a positive correlation between VEGFA and hepatic fibrosis was observed in the NAFLD-HCC cohort, but not in the HBV-HCC cohort. Moreover, LX2 cells could be activated by conditioned medium from NAFLD-derived organoids, but not from HBV livers, whereas this activation was blocked by a VEGFA antibody. In summary, our findings reveal that hepatocyte-derived VEGFA contributes to NAFLD-HCC development by activating HSCs and highlight the potential of precisely targeting hepatocytic VEGFA as a promising therapeutic strategy for NAFLD-HCC.

Keywords: VEGFA; NAFLD; HCC; fibrosis; hepatic stellate cells

Acta Pharmacologica Sinica (2022) 43:2917–2928; https://doi.org/10.1038/s41401-022-00907-5

INTRODUCTION

Over the last decade, non-alcoholic fatty liver disease (NAFLD) has become the most common cause of chronic liver disease worldwide owing to the obesity pandemic. NAFLD is present in 25% of the world's population and represents a wide spectrum of diseases, ranging from simple steatosis to non-alcoholic steatohepatitis (NASH) to cirrhosis [1]. Although most patients with NAFLD have only steatosis without progression, more than one-third of NAFLD cases develop NASH, which may cause fibrosis, cirrhosis, and hepatocellular carcinoma (HCC) [2]. Despite the growing public health impact of NAFLD, therapeutic options remain limited [1] owing to the indistinct mechanisms.

The progression of NAFLD to HCC is characterized by inflammation, fibrosis, and pathological angiogenesis [3, 4]. This progression is closely associated with a series of injuries that constitutes the "second hit" [5]. Defective hepatocyte regeneration, which is important for the replenishment of dead cells, has been proposed as the "third hit" in NAFLD development [6]. These hepatic injuries eventually lead to the activation of HSCs, collagen and extracellular matrix deposition, consequently promoting fibrosis and cirrhosis [7]. A wide range of pathological conditions requires a strong pathophysiological dialogue between different populations of liver cells.

Pathological angiogenesis appears to be intrinsically associated with fibrogenesis during chronic liver disease progression. Vascular endothelial growth factor A (VEGFA), a key regulator of angiogenesis, is involved in endothelial dysfunction and immune cell infiltration in chronic liver diseases [8, 9]. Liver VEGFA is secreted by hepatic stellate cells (HSCs), Kupffer cells, and hepatocytes to regulate the LSEC phenotype [10–12]. Previous studies have identified the deleterious role of excess VEGFA levels in liver tumorigenesis. Thus, numerous anti-angiogenic molecules are currently being used as treatment options for liver cancer [13]. However, some clinical data have shown conflicting evidence regarding VEGFA alteration in the progression of NAFLD [14–16]. A general analysis of the correlation between VEGFA and NAFLD is possibly mixed because VEGFA from different cell sources is likely to have a different impact on metabolic diseases. However, the

[1]International Cooperation Laboratory on Signal Transduction, National Center for Liver Cancer, Ministry of Education Key Laboratory on signaling Regulation and Targeting Therapy of Liver Cancer, Shanghai Key Laboratory of Hepato-biliary Tumor Biology, Eastern Hepatobiliary Surgery Hospital, Second Military Medical University/NAVAL Medical University, Shanghai 200433, China; [2]Department of Pathology, Shanghai Tenth People's Hospital, Tongji University School of Medicine, Shanghai 200072, China; [3]Institute of Metabolism and Integrative Biology, Fudan University, Shanghai 200438, China and [4]Third Department of Hepatic Surgery, Eastern Hepatobiliary Surgery Hospital, Second Military Medical University, Shanghai 200433, China
Correspondence: Hong-yang Wang (hywangk@vip.sina.com) or Yao Chen (chyyn2003@163.com)
These authors contributed equally: Hao Shen, Han Yu, Qian-yu Li, Ya-ting Wei

Received: 15 December 2021 Accepted: 2 April 2022
Published online: 4 May 2022

role of VEGFA in the progression of NAFLD to steatohepatitis, advanced fibrosis, and HCC remains unclear. Therefore, it is essential to distinguish VEGFA from other potential cellular sources and determine its distinct role during the different stages of the NAFLD process.

In this study, we found progressive accumulation of VEGFA, especially in hepatocytes, in patients or mice with NAFLD-HCC. Mice with VEGFA deficiency in hepatocytes were used to determine the exact role of hepatocyte-derived VEGFA in this specific pathological transition. The present study provides primary evidence of the deleterious role of hepatocyte-derived VEGFA in mediating HSC activation to promote NAFLD-HCC progression.

MATERIALS AND METHODS

Generation of hepatocyte-specific deficiency of VEGFA mice and treatments

Vegfa$^{fl/fl}$ mice were a gift from Genentech (South San Francisco, CA, USA), and crossed with liver-specific *Cre* (albumin, *Alb-Cre*) mice to generate *Alb-Vegfa* mice (*Vegfa*$^{\Delta hep}$). C57BL/6 wild type (WT) mice were purchased from Shanghai Model Organisms Center, Inc. (Shanghai, China). All the mice (8 weeks old) were maintained in filter-topped cages on an autoclaved normal chow diet (ND) and normal tap water or western diet (WD, composed of 21.1% fat, 41% sucrose, and 1.25% cholesterol by weight, Shanghai Fanbo, No. 170092) and a high sugar solution (23.1 g/L d-fructose and 18.9 g/L d-glucose). Carbon tetrachloride (CCl_4) at a dose of 0.2 μL (0.32 μg)/g of body weight, or its control (olive oil), was injected intraperitoneally once weekly, starting simultaneously with the diet administration. Experimental groups were as follows: ND/CCl_4-WT, $n = 5$; WD/CCl_4-WT, 0 ($n = 5$), 12 weeks ($n = 5$), 24 ($n = 8$) and 36 ($n = 16$) weeks; ND/CCl_4-*Vegfa*$^{\Delta hep}$, $n = 5$; WD/CCl_4-*Vegfa*$^{\Delta hep}$, 0 ($n = 5$), 12 ($n = 5$), 24 ($n = 8$) and 36 ($n = 16$) weeks. Rescue experiments were performed by tail vein injection of lentivirus-delivered VEGFA (5×10^7 per mouse, $n = 5$) or control into *Vegfa*$^{\Delta hep}$ at 6 weeks old, which received WD/CCl_4 treatment at 8 weeks for the indicated time. The mice were sacrificed at the indicated times by exsanguination after anaesthesia. Liver and serum samples were collected and processed for histological, serological, and other analysis.

Clinical liver specimens

Clinical specimens were obtained from the Eastern Hepatobiliary Surgery Hospital (EHBH) in Shanghai with the approval of the EHBH Research Ethics Committee. NAFLD-related HCC samples were collected under the following conditions: (1) fatty liver diagnosed by imaging studies (including CT, MRI, or ultrasound); (2) no history of heavy alcohol consumption or viral hepatitis; and (3) hepatic resection for liver tumor. Samples of hepatitis B (HBV)-related HCC were collected: (1) without a clinical diagnosis of NAFLD, (2) with HBV infection, and (3) received hepatic resection for liver tumor. The samples of hepatic haemangioma were collected as follows: (1) without clinical diagnosis of NAFLD or HBV infection and (2) underwent hepatic resection for hepatic haemangioma. After surgical excision, liver tissues were collected from the peri-tumor region as far as possible from the lesion.

Real-time PCR

Total RNA was extracted from cells and tissues using TRIZOL Reagent (Invitrogen, Waltham, MA, USA) and reverse-transcribed using the M-MLV system (Promega, Madison, WI, USA). For real-time PCR, SYBR Green PCR Master Mix (Roche, Basil, Switzerland) and LightCycler® 96 (Roche) were used to conduct the experiments. The primers used for the genes are listed in Supplementary Table 1.

Western blot and ELISA assay

Blotting was performed according to standard procedures. Antibodies are listed as follows: α-SMA (1:1000; abcam; No. 7817), TIMP-1 (1:1000; abcam; No. 211926), VEGFA (1:1000; abcam; No. 52917), p53BP1 (1:1000; abcam; No. 175933), 8-OHdG (1:500; Bioss; No. 1278), p-H2A.X (1:1000; abcam; No. 26350), Cyclin D1 (1:1000; Proteintech; No. 60186), PCNA (1:1000; abcam; No. 29), GAPDH (1:1000; Cell signaling technology; No. 8884S) and the fluorescein-conjugated secondary antibody (1:10000; LI-COR; No. 926–32210 and 926–32211). Odyssey fluorescence scanner (Li-Cor, Lincoln, NE) was used to record the images. VEGFA levels in serum or liver tissues were measured by ELISA kit (Dakewe Bio-engineering; No. 1117342 (human) and 1217342 (mouse)) according to the manufacturer's instructions.

Reactive oxygen species and antioxidant detection

The levels of reactive oxygen species (ROS) and reactive nitrogen species (RNS) in murine liver tissues were analysed using a DCF ROS/RNS assay kit (abcam, No. 238535). An ultrasensitive assay for glutathione in the samples was performed using a GSH/GSSG ratio detection assay kit (abcam, No. 138881).

Immunohistochemical/Periodic Acid-Schiff (PAS)/Sirius red/Oil red O staining/TUNEL staining

Liver tissues embedded in paraffin were cut into 5 μm-thick sections. All the slides were photographed using a Leica Aperio AT2 400 microscope (Leica, Germany) and images were analysed using Aperio ImageScope (v12.3.2.7001).

Sections were incubated with VEGFA (1:250; abcam; No. 185238) antibodies at 4 °C overnight, horseradish peroxidase-conjugated secondary antibody (Supervision; No. D-3001 and D-3002) at 37 °C for 1 h, and immunoreactive cells were visualized using DAB. Counterstaining was performed with haematoxylin.

For PAS staining, the tissue sections were de-paraffinised and hydrated in water followed by oxidization in 0.5% periodic acid solution for 5 min. After rinsing in distilled water, the slides were placed in Schiff's reagent for 15 min and counterstained with haematoxylin for 1 min.

The Sirius red/fast green collagen staining kit (Chondrex. Inc, No. 9046), Oil Red O kit (abcam, No. 150678) and TUNEL staining kit (UE EVERBRIGHT Inc, No. T6068) was conducted according to previously published protocols, respectively.

Immunofluorescence

Paraffin-embedded sections were incubated with anti-VEGFA (1:500; abcam; No. 185238), anti-α-SMA (1:3000; abcam; No. 7817) or anti-E-cadherin (1:400; Cell Signaling Technology; No. 3195) at room temperature for 2 h after blocking with 1% BSA and 10% goat serum. The sections were then treated with the TSA plus fluorescence kit (PerkinElmer, No. NEL752001KT and NEL741001KT) following the standard protocol. Images were obtained using a laser scanning confocal microscope (Leica TCS SP8, Germany).

Glucose tolerance test (GTT)

A GTT was performed according to standard procedures. First, the mice were fasted with only a water supply the day before the experiment. Mice were then intraperitoneally injected with a 10% glucose solution (2 mg glucose/g body weight). Blood glucose levels were measured at 30, 60, 90 and 120 min, and the data were collected and are shown in a line chart.

Isolation of primary hepatocyte

Primary hepatocytes were isolated using a two-step perfusion method as previously described [17]. Briefly, isolated hepatocytes were cultured on collagen-coated culture dishes and used

for experiments on the following day. Clinical specimens for primary hepatocyte isolation were obtained according to the ethical guidelines of our hospital, and written informed consent was obtained from patients for the use of tissue for research purposes.

Hepatic organoid culture

Organoid culture was based on the protocol reported by Broutier et al. [18]. Briefly, under aseptic conditions, the tissues were placed in a 100-mm Petri dish and minced into pieces of ~0.5–1 mm^3. The minced tissues were washed twice in ice-cold organoid basal medium and incubated with digestion solution (2.5 mg/mL, collagenase VI (Sigma, No. C5138) and 0.1 mg/mL, DNase I (Sigma, No. D5025)) at 37 °C for 45–60 min until all tissues were digested. The mixture of tissues and digestion solution was passed through a 70 μm strainer (Falcon). Hepatocytes were separated from nonparenchymal cells (NPCs) by low-speed centrifugation (800 rpm × 5 min × 3), and further purified by Percoll gradient centrifugation (50% *v/v*, Sigma, No. P4937). Human hepatocyte organoids were cultured with a series of STEMCELL products according to the protocols: HepatiCult Organoid Basal Medium (Human) (STEMCELL 100–0386), Growth Supplement (Human) (100–0389), Differentiation Supplement (Human) (100–0388). The supernatant was collected for the assays or stimulation.

LX2 cells culture and treatment

Human LX2 cells were cultured in DMEM with 10% fetal bovine serum (FBS, Gibico Life Technologies, Grand Island, NY), 1% (*v/v*) sodium pyruvate, 1% (*v/v*) glutamine and 1% (*v/v*) penicillin/streptomycin at 37 °C in 5% CO_2 and 95% air-humidified incubator. LX2 cells (1×10^5) were seeded in 24-well plates for 24 h and then exposed to human recombinant VEGFA (50 nM; PeproTech; No. 1002010) with or without pretreatment with palmitic acid (PA, 0.5 mM) and oleic acid (OA, 1 mM). LX2 cells were also exposed to the collected supernatant from the organoids pretreated with PA and OA for 2 days. The VEGFA neutralization antibody (2 μg/ml; R&D; No. AF-493-NA), mouse IgG (R&D; No. AB-108-C) as the control, or the VEGFR inhibitor Axitinib (0.3 nM; Selleck; No. S1005) was selectively added to the conditioned medium.

Statistical analysis

All values presented are expressed as mean ± SD or median ± quartiles (if the value is non-normally distributed). The χ^2 test and Student's *t* test were used to determine the statistical significance. One-way ANOVA followed by Tukey's multiple comparison test was used to compare three or more groups. The Pearson correlation coefficient was calculated for the two variables. Differences were considered significant at $P < 0.05$ (*$P < 0.05$; **$P < 0.01$; ***$P < 0.001$). Data analysis was performed using SPSS software (version 16; SPSS).

RESULTS

Hepatic VEGFA levels were elevated considerably in hepatocytes during NAFLD-HCC transition

To investigate the relevance of VEGFA in NAFLD-HCC progression, we first examined the expression of VEGFA in patients with NAFLD in two different cohorts from the Gene Expression Omnibus Datasets (GSE130970 and GSE135251). VEGFA levels were increased in NAFLD tissues of the "GSE130970 cohort", in which all biopsies were graded according to the SAF scoring system and disease severity was classified as 0–4 grade (Fig. 1a, left). Similarly, VEGFA levels were elevated in early or moderate NAFLD tissues compared with control in the "GSE135251 cohort" (Fig. 1a, right). Furthermore, in our HCC cohort (Table 1), serum VEGFA levels were significantly higher in HCC patients with NAFLD background than in those non-NAFLD (Fig. 1b). In the liver tissue sections, immunohistochemical staining for VEGFA was also significantly higher in the patients with NAFLD (Fig. 1c). Interestingly, confocal images of E-cadherin revealed abundant VEGFA-positive hepatocytes in NAFLD tissues and a small proportion of other hepatic cells in non-NAFLD tissues (Fig. 1d). Moreover, primary hepatocytes isolated from NAFLD-HCC tissues showed much higher levels of VEGFA than those isolated from non-NAFLD-HCC tissues (Fig. 1e).

Next, we established a murine NAFLD-HCC model, which was induced by WD combined with CCl_4 (WD/CCl_4), as previously described (Fig. 1f) [19]. As shown in Fig. S1a, WD/CCl_4 mice showed significant weight gain and adiposity compared to ND/CCl_4 mice (Fig. S1a), and higher blood glucose levels (Fig. S1b) but less glycogen deposition in the liver tissue (Fig. S1c) at 24 and 36 weeks compared with ND/CCl_4 mice, indicating dysregulated glucose metabolism. Accordingly, the WD/CCl_4 mice showed aberrant liver lipid metabolism, including significantly increased serum and liver triglycerides, total serum cholesterol, serum free fatty acids (FFAs) and hepatic lipid accumulation (Fig. S1c–e). Based on the grade of steatosis, ballooning, lobular inflammation and fibrosis, WD/CCl_4 mice had a higher SAF score at 36 weeks than the control mice (Fig. S1d). Consistently, WD/CCl_4-WT mice showed elevated serum alanine aminotransferase (ALT) and aspartate aminotransferase (AST) levels, accompanied by increased ROS production and a decreased GSH/GSSG ratio (Fig. S1f), indicating serious hepatic injury. In contrast to ND/CCl_4 mice, 12.5% (1/8) and 100% (8/8) WD/CCl_4 mice exhibited massive nodules at 24 and 36 weeks, respectively (Fig. S1g). Collectively, these data confirmed the murine NAFLD-HCC model with rapid progression of advanced fibrosis and HCC, sharing classic features of common human NAFLD development and faithfully recapitulating the natural history of chronic damage, inflammation, fibrosis, and HCC (Fig. S1). We used this murine NAFLD-HCC model to explore the role of VEGFA in this process.

VEGFA protein levels in liver, rather than in serum, gradually increased during NAFLD (Figs. 1g, h, S1h). When NAFLD formed at 12 weeks, some VEGFA-positive hepatocytes appeared in liver, which further increased to 15% and 35% at 24 and 36 weeks, respectively (Fig. 1h). Most of the VEGFA-positive hepatocytes were distributed in the portal and periportal areas (Fig. 1h). Immunofluorescence staining of E-cadherin and VEGFA further confirmed that VEGFA was significantly increased in the hepatocytes of WD/CCl_4 mice (Fig. 1i). In contrast, very few hepatocytes were VEGFA-positive in the ND/CCl_4 mice (Fig. 1i). Consistently, VEGFA levels in isolated mouse hepatocytes gradually increased with WD/CCl_4 treatment in a time-dependent manner (Fig. 1j).

Combining the experimental murine NAFLD-HCC model with the clinical data, we hypothesize that hepatocyte-derived VEGFA promotes NAFLD-HCC development.

Hepatocyte-derived VEGFA promoted fibrosis rather than hepatic steatosis

To test our hypothesis, we crossed *Vegfa*$^{fl/fl}$ mice with *Albumin-Cre* mice to generate hepatocyte-specific deletion of VEGFA mice (*Vegfa*$^{\Delta hep}$) and treated them with ND/CCl_4 or WD/CCl_4 as previously described (Fig. 2a). *Vegfa*$^{\Delta hep}$ mice developed normally and had a lifespan similar to that of WT mice did. *Vegfa*$^{\Delta hep}$ livers were normal in size and had the same hierarchical microvasculature of liver sinusoids as that of WT mice (Fig. S2a). In the ND/CCl_4 condition, serum and liver triglycerides, total serum cholesterol, and serum free fatty acids were not significantly different between the WT and *Vegfa*$^{\Delta hep}$ groups (Fig. S2b), indicating a small difference in the lipid metabolism. AST levels did not differ between the two groups, despite the decrease in ALT levels in ND/CCl_4-*Vegfa*$^{\Delta hep}$ mice at 36 weeks (Fig. S2c). Under NAFLD conditions, WD/CCl_4-*Vegfa*$^{\Delta hep}$ mice showed few VEGFA-positive hepatocytes (Fig. 2b, c) and almost entirely deficient

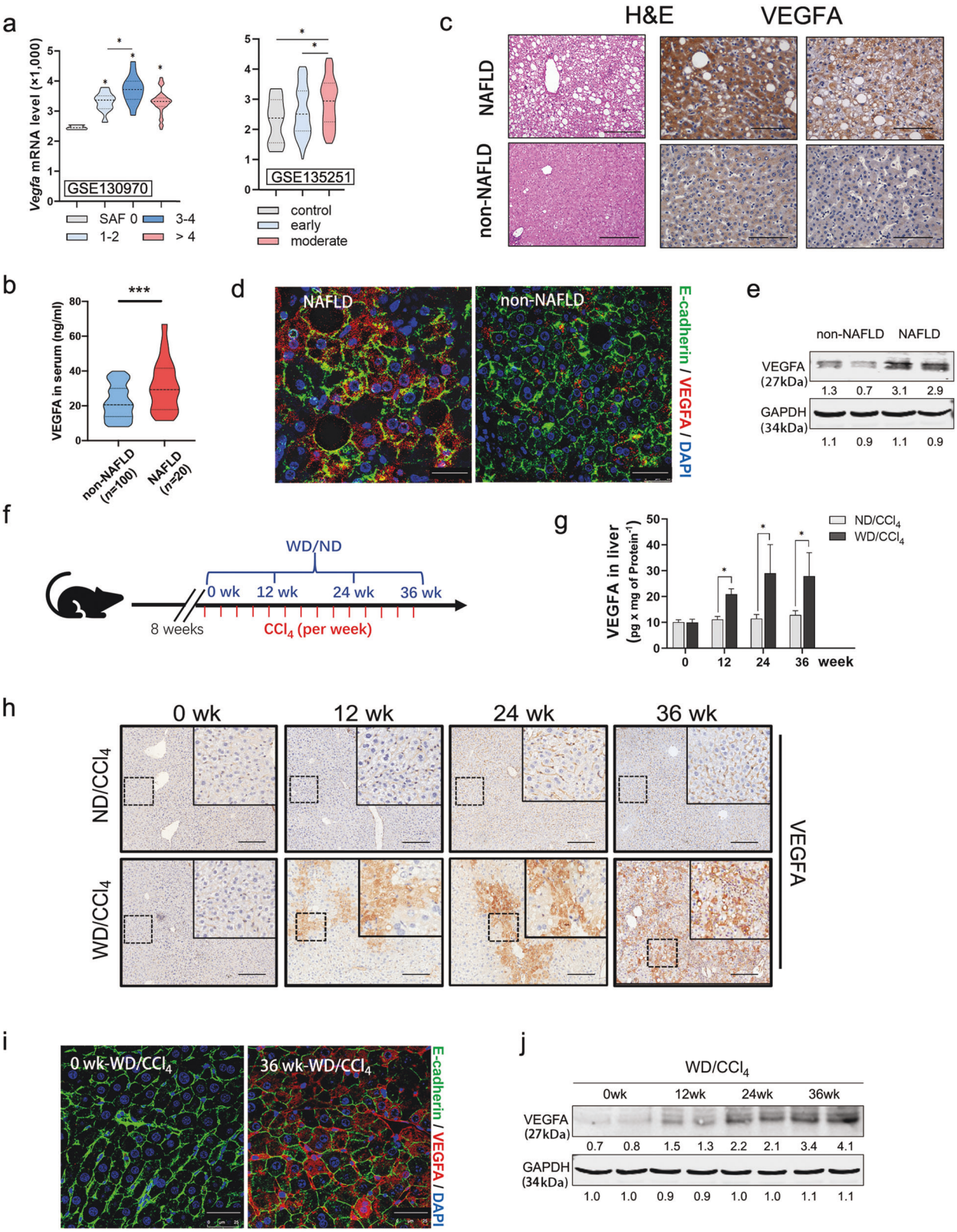

expression in isolated hepatocytes (Fig. 2d) during the NAFLD-HCC transition. Both WD/CCl_4-WT and WD/CCl_4-*Vegfa*$^{\Delta hep}$ mice displayed a steady increase in body weight and no difference in the liver-to-body weight ratio before 24 weeks (Figs. 2e, S3b). No significant differences in glucose tolerance, glycogen deposition and hepatic lipid accumulation were observed in two groups at 24 weeks (Fig. 2f–h). However, WD/CCl_4-*Vegfa*$^{\Delta hep}$ mice exhibited lower serum levels of ALT and AST (Fig. 2i) and lower levels of ROS (Fig. S3e, f). Notably, WD/CCl_4-*Vegfa*$^{\Delta hep}$ displayed less fibrosis and collagen deposits compared to WT mice at 24 weeks (Fig. 2j, k),

Fig. 1 Hepatic VEGFA increased considerably in hepatocytes during NAFLD-HCC progression. a Violin plot analysis presented the mRNA levels of VEGFA in two NAFLD cohorts from GEO Datasets (GSE13097, GSE135251). According to the SAF score, disease severity was classified as 0–4 grade (GSE13097) or early/moderate degree (GSE135251). VEGFA mRNA expression was evaluated in these subjects. The middle dashed line represents the median value; upper and lower dashed lines represent the quartiles. **b** Serum levels of VEGFA in HCC patients with ($n = 20$) or without ($n = 100$) NAFLD were determined by ELISA assay. Data were represented as median ± quartiles, compared using Student's t test with Welch's correction. **c** Representative H&E and immunohistochemical staining of VEGFA in peri-tumorous tissues from patients with or without NAFLD. Scale bars, 100 μm. **d** Representative fluorescent microscopy of VEGFA expression in patients with or without NAFLD. Hepatocytes were immunostained by E-cadherin (green), and the nucleus by DAPI (blue). Scale bars, 25 μm. **e** VEGFA protein levels in primary hepatocytes from patients with or without NAFLD were determined by Western blot. GAPDH was used as a loading control. **f** Scheme depicting experimental outline of mice treated with diet and CCl_4. At age of 8 week, mice were treated with normal diet combined with carbon tetrachloride (ND/CCl_4) or western diet combined with carbon tetrachloride (WD/CCl_4) for the indicated time. **g** ELISA analysis of VEGFA expression in the liver tissues from ND/CCl_4 or WD/CCl_4 mice (ND/CCl_4, $n = 5$; WD/CCl_4-WT, 0 week $n = 5$, 12 weeks $n = 5$, 24 weeks $n = 8$, and 36 weeks $n = 16$). Data were represented as mean ± S.D. **h** Representative hepatic VEGFA staining in ND/CCl_4- or WD/CCl_4-WT livers at indicated time. Scale bars, 100 μm. **i** Representative fluorescent microscopy of VEGFA expression in WD/CCl_4-WT liver. Hepatocytes were immunostained by E-cadherin (green), and the nucleus by DAPI (blue). Scale bars, 25 μm. **j** Protein levels of VEGFA in primary hepatocytes of WD/CCl_4-WT mice at indicated time were determined by Western blot. GAPDH was used as a loading control. $^*P < 0.05$, $^{***}P < 0.001$.

Table 1. Clinical characteristics of HCC patients with/without NAFLD.

Characteristic	Non-NAFLD HCC ($n = 100$)	NAFLD HCC ($n = 20$)	P value
Age, year	51.3 (43.2–58.0)	52.6 (39.5–64.2)	0.4778
Gender, male, n (%)	81 (81)	16 (80)	NA
Body mass index	21.3 (18.6–25.3)	24.0 (22.6–27.2)	0.0033**
AFP, ng/mL	7.9 (3.0–104.8)	6.8 (2.4–25.4)	0.4353
ALT, U/L	33.0 (22.0–47.2)	31.0 (22.6–39.8)	0.9096
AST, U/L	30.0 (21.9–43.2)	35.0 (17.3–49.5)	0.6993
ALB, g/L	40.3 (37.9–43.7)	42.1 (39.2–43.0)	0.6650
TBIL, μmol/L	18.6 (14.6–26.3)	18.5 (12.9–33.6)	0.8847
DBIL, μmol/L	9.6 (7.2–13.9)	8.6 (5.9–15.5)	0.5394
GGT, U/L	74.0 (49.3–121.4)	84.4 (52.7–139.3)	0.9727
ALP, U/L	92.0 (78.5–132.0)	78.8 (72.4–96.6)	0.0942

Results are expressed as median (interquartile range). T test, Kruskal–Wallis and Chi-Square tests were used to compare patient characteristics.
AFP alpha-fetoprotein, *AST* Aspartate Aminotransferase, *ALT* Alanine Aminotransferase, *ALB* albumin, *TBIL* total bilirubin, *DBIL* direct bilirubin, *GGT* γ-glutamyltransferase, *ALP* alkaline phosphatase.
$^{**}P < 0.01$ for P values shown in the table.

which was further confirmed by the SAF score (3.2 ± 0.4 vs. 1.8 ± 0.4, $P < 0.05$) (Fig. 2l). In contrast, lentivirus-mediated overexpression of VEGFA aggravated liver fibrosis in *Vegfa*$^{\Delta hep}$ mice at 24 weeks (Fig. S4a–e). Together, these results indicate that hepatocyte-derived VEGFA mainly promotes liver fibrosis rather than steatosis during the NAFLD-HCC transition.

Hepatocyte-derived VEGFA exacerbated liver injury and accelerated NAFLD-HCC transition

In the WD/CCl_4-induced NAFLD-HCC model, 12.5% of the WT mice showed visible liver nodules at 24 weeks whereas none of the *Vegfa*$^{\Delta hep}$ mice did (Fig. S3a). At 36 weeks, all of WD/CCl_4-WT mice showed nodules with greater numbers and larger sizes, whereas 50% of WD/CCl_4-*Vegfa*$^{\Delta hep}$ mice had fewer nodules with smaller sizes (Fig. 3a, b). Haematoxylin and eosin staining confirmed that these nodules were histopathological tumor lesions (Fig. 3c), in which positive immunostaining for CD31 and TUNEL staining were observed (Fig. S3c, d). Although the tumors lesions were coherently characterized by AFP immunostaining (Fig. 3d), *Vegfa*$^{\Delta hep}$ mice had lower levels of ALT and AST and less ROS at 36 weeks (Fig. 3e, f), implying relatively mild hepatic injury. Consistently, *Vegfa*$^{\Delta hep}$ mice showed not only less nuclear staining of DNA damage markers, 8OHdG and p53BP1 (Fig. 3g), but also lower protein levels of p53BP1 and p-H2A.X (Fig. 3h) in tumor tissues compared to those of WT mice. Moreover, the protein levels of cyclin D1 and PCNA and immunostaining of Ki67 and CD31, except for TUNEL staining, were reduced in tumor tissues of *Vegfa*$^{\Delta hep}$ mice, indicating an alleviative malignancy (Figs. 3h, i, S3c, d). Furthermore, overexpression of *Vegfa* in the liver led to visible lesions in *Vegfa*$^{\Delta hep}$ mice at 24 weeks (Fig. S4f, g). Together, these results strongly suggest that hepatocyte-derived VEGFA exacerbates hepatic injury and promotes the NAFLD-HCC transition.

Hepatocyte-derived VEGFA promoted endothelial dysfunction and activated HSCs during NAFLD-HCC transition

VEGFA is involved in pathological angiogenesis and plays an important role in liver fibrosis development [10, 20]. Pathological angiogenesis and fibrosis are crucial for the progression of NAFLD [21]. To exclude the confounding effect of tumors, liver tissues from 24 weeks were analysed between the two groups. In *Vegfa*$^{\Delta hep}$ livers, the number of CD31-positive cells was significantly lower than in WT mice, suggesting a lower density of micro-vessels (Fig. 4a). In addition, the endothelial dysfunction markers ICAM-1 and VCAM-1, were downregulated in *Vegfa*$^{\Delta hep}$ mice (Fig. 4b, c). The composition of infiltrating immune cell subsets is altered in experimental NAFLD pathogenesis [22]. We found significant downregulation of *Cd8* and *Cd4* in *Vegfa*$^{\Delta hep}$ mice compared to those in WT mice, whereas no significant differences in *Cd11b* and *F4/80* were observed between the two groups (Fig. S3e).

HSCs are the dominant contributors to NASH liver fibrosis and profoundly alter the tumor microenvironment [23]. In our NAFLD-HCC model, the mRNA levels of α-SMA, *Tgfb1, Timp1, Col1a1 and Mmp2*, were significantly downregulated in the livers of *Vegfa*$^{\Delta hep}$ mice (Fig. 4d). Consistently, the liver protein levels of α-SMA and TIMP1 were remarkably reduced in *Vegfa*$^{\Delta hep}$ mice (Fig. 4e). Notably, confocal images showed the close proximity of α-SMA-positive HSCs and VEGFA-positive hepatocytes in WT livers, but not in *Vegfa*$^{\Delta hep}$ livers (Fig. 4f). To determine the effect of VEGFA on HSCs in vitro, LX2 human HSC line were stimulated with VEGFA in the presence or absence of PA (0.5 mM) and OA (1 mM). Remarkably, in the presence of PA and OA, VEGFA significantly stimulated LX2 into a fibrogenic phenotype with upregulation of α-SMA, TGFB1 and TIMP1 (Fig. 4g, h). Moreover, treatment with VEGFA antibody (α-VEGFA) or the VEGFR inhibitor Axitinib (VEGFR inh) evidently attenuated the fibrogenic phenotype of LX2 (Fig. 4i, j), indicating VEGFA-VEGFR signal involvement in VEGFA function. Collectively, these results suggest that, in addition to exacerbated endothelial dysfunction, hepatocyte-derived VEGFA activates HSCs to promote NASH fibrosis in NAFLD-HCC development.

Hepatic VEGFA levels were positively correlated with fibrosis mainly in NAFLD- but not in HBV-patients

Although HBV and NAFLD are the independent risk factors for fibrosis progression and cirrhosis, both have high prevalence in Asia [24]. Concurrent HBV was found in 28.57% of the NAFLD patients [25]. Concomitant NAFLD in patients with chronic

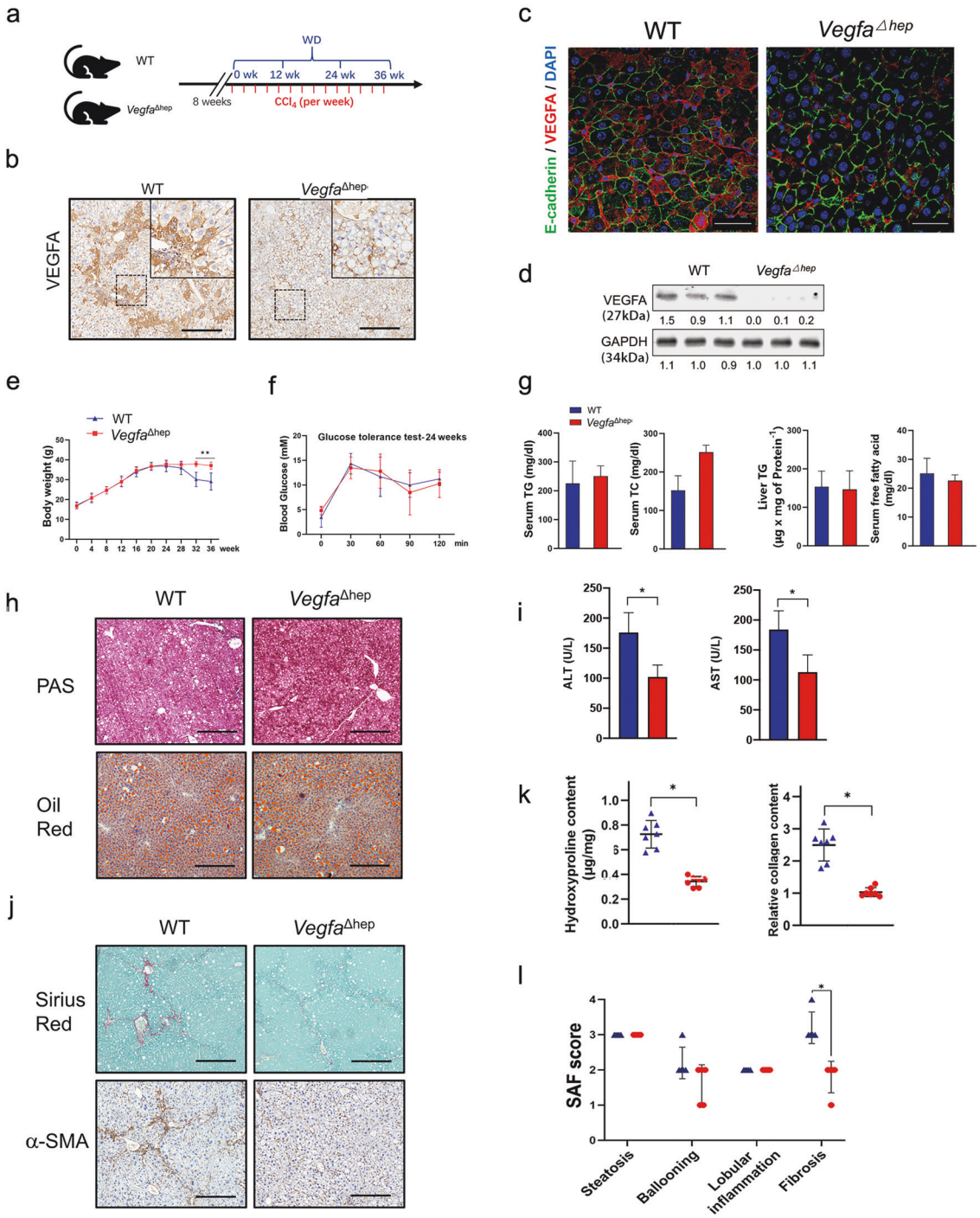

Fig. 2 Hepatocytic deletion of VEGFA alleviated liver fibrosis but not steatosis in WD/CCl_4 mice. a Scheme depicting experimental outline of WT or *Vegfa*$^{\Delta hep}$ mice treated with WD/CCl_4. **b** Immunohistochemical staining of VEGFA in liver section from WD/CCl_4-WT and -*Vegfa*$^{\Delta hep}$ mice at 24 weeks. Scale bars, 100 μm. **c** Representative fluorescent microscopy of VEGFA expression in WD/CCl_4-WT or WD/CCl_4-*Vegfa*$^{\Delta hep}$ mice at 24 weeks. Hepatocytes were immunostained by E-cadherin (green), and the nucleus by DAPI (blue). Scale bars, 25 μm. **d** Protein levels of VEGFA in primary hepatocytes from WD/CCl_4-WT or -*Vegfa*$^{\Delta hep}$ mice at 24 weeks. GAPDH was used as a loading control. **e** Body weight change record for 36 weeks ($n = 16$). **f** Glucose tolerance test was performed at 24 weeks ($n = 8$). **g** Serum and liver TG, serum TC, and FFAs concentrations were determined. Data are represented as mean ± SD. **h** Representative PAS, Oil Red staining in WD/CCl_4-WT and -*Vegfa*$^{\Delta hep}$ mice at 24 weeks. Scale bars, 300 μm. **i** Serum AST and ALT concentrations in both mice at 24 weeks ($n = 8$). Data are represented as median ± quartiles. **j** Representative Sirius Red and α-SMA staining at 24 weeks. Scale bars, 300 μm. **k** Hydroxyproline assay (left) and tissue collagen assay (right). **l** SAF score showed the disease severity of NAFLD in both groups. *$P < 0.05$, **$P < 0.01$.

hepatitis B (CHB) has a higher fibrosis stage than in those without CHB. Given the role of VEGFA in fibrosis, we further compared the clinical NAFLD- and HBV-related fibrosis samples, which were peri-tumor specimens with advanced fibrosis, based on the diagnostic criteria and clinicopathological data (Table 2). There was no statistical difference in VEGFA levels between the NAFLD- and HBV-related fibrosis groups (Fig. 5a). Sirius red staining showed a large amount of collagen deposition in both

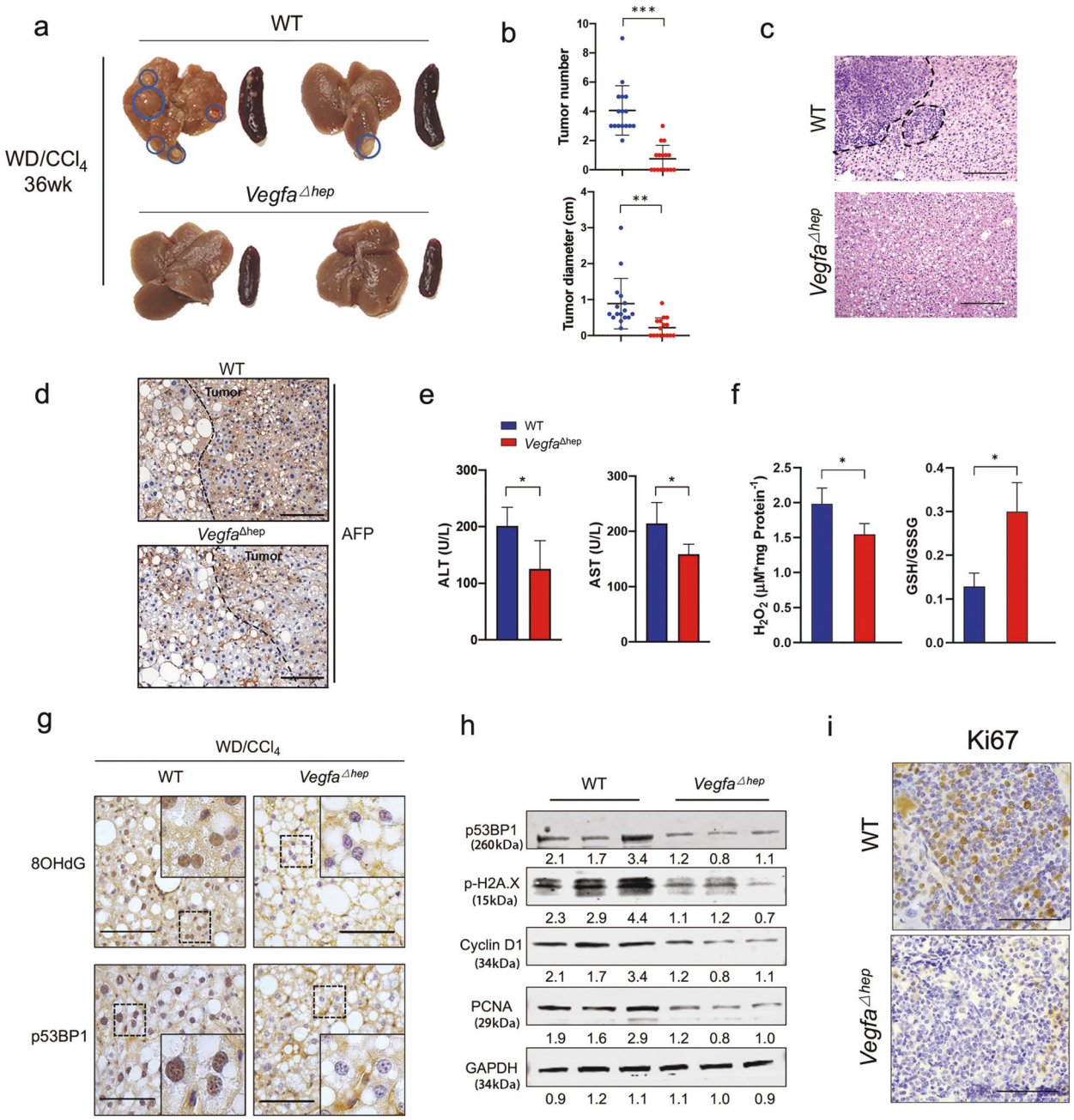

Fig. 3 Hepatocyte-derived VEGFA aggravated liver injury and accelerated NAFLD-HCC transition. a The representative livers and spleens from WD/CCl_4-WT and -*Vegfa*$^{\Delta hep}$ mice at 36 weeks. **b** Quantification of the tumor number, tumor size of both mice (**a**) ($n = 16$). **c** Representative H&E image of WD/CCl_4-WT or -*Vegfa*$^{\Delta hep}$ livers at 36 weeks. Scale bars, 300 μm. **d** Representative immunohistochemical staining of AFP in tumor section in (**a**). Scale bars, 100 μm. **e** Serum AST and ALT concentrations from (**a**). Data are represented as median ± quartiles. **f** The ROS level and GSH/GSSG ratio in peri-tumor liver tissues in (**a**). **g** Immunohistochemical staining of 8OHdG and p53BP1 in peri-tumor liver section. Scale bars, 25 μm. **h** Protein expressions of p53BP1, p-H2A.X, Cyclin D1, and PCNA were determined in liver tumor tissues. **i** Immunohistochemical staining of Ki67 in liver tumor section (**a**). Scale bars, 25 μm. *$P < 0.05$, ***$P < 0.001$.

groups, but no statistical significance was observed in the fibrosis score (Fig. 5b, c). Interestingly, there was a certain degree of correlation between VEGFA and liver fibrosis-related genes, *α-SMA, TGFB1, TIMP1 and MMP2*, in the NAFLD group, but not in the HBV group (Figs. 5d, S5a). It should be noted that numerous VEGFA-positive hepatocytes and adjacent activated HSCs were visible in NAFLD-fibrotic tissues (Fig. 5e). Intriguingly, activated HSCs adjacent to VEGFA-positive nonparenchymal cells were distributed in the HBV-fibrosis group (Fig. 5e). These results indicate that hepatocellular VEGFA is a risk factor for NAFLD fibrosis.

Hepatocyte organoids derived from NAFLD specimens stimulated HSCs activation via VEGFA secretion

Patient-derived hepatocytes were explored to generate organoids and were applied to model chronic liver diseases to understand the pathological mechanisms [18]. A small portion of VEGFA-positive other hepatic cells adjacent to activated HSCs was also distributed in the HBV-fibrosis specimens (Fig. 5e). To exclude the complex effects of mixed nonparenchymal cells on HSCs in vivo, we used an organoid culture system to explore the effect of VEGFA on HSCs activation (Fig. 6). Liver tissues were collected from seven patients with NAFLD, twelve with HBV-fibrosis, and four with

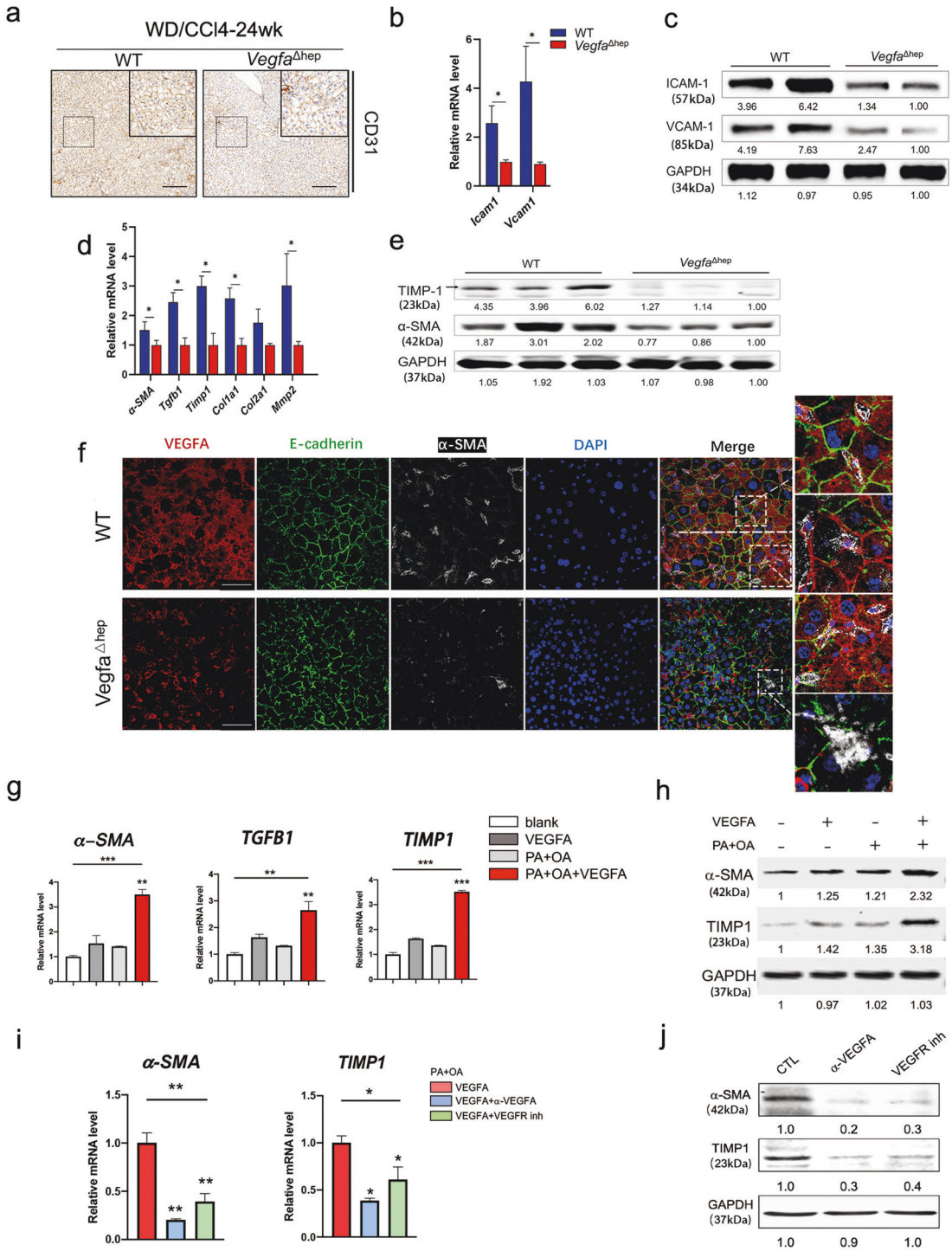

Fig. 4 Hepatocyte-derived VEGFA promoted endothelial dysfunction and activated HSCs during NAFLD-HCC transition. a Representative immunohistochemical staining of CD31 in WD/CCl_4-WT and -*Vegfa*$^{\Delta hep}$ livers at 24 weeks. Scale bars, 100 μm. **b**, **c** RNA and protein expression of endothelial dysfunction markers in WD/CCl_4-WT and -*Vegfa*$^{\Delta hep}$ mice were measured by real-time PCR (**b**) and Western blot (**c**). ($n = 8$). Data are represented as mean ± SD. **d**, **e** RNA (**d**) and protein expression (**e**) of activated HSCs markers in WD/CCl_4-WT and -*Vegfa*$^{\Delta hep}$ mice were measured. ($n = 8$). **f** Immunofluorescence analyses of VEGFA expression and HSCs activation in WD/CCl_4-WT and -*Vegfa*$^{\Delta hep}$ mice at 24 weeks. Activated HSCs were immunostained by α-SMA. Scale bars, 25 μm. **g**, **h** Relative RNA (**g**) and protein (**h**) levels of activated HSCs-related markers in LX2 treated with VEGFA (50 nM), PA (0.5 mM) + OA (1 mM), VEGFA + PA + OA, versus with Vehicle control for 24 h, respectively. **i**, **j** Relative RNA (**i**) and protein (**j**) levels of activated HSCs-related markers in LX2, which was pretreated with VEGFA + PA + OA, then treated with α-VEGFA (2 μg/mL) or VEGFR inhibitor Axitinib (0.3 nM, VEGFR inh), respectively. One-way ANOVA followed by Tukey's test was used for multiple comparisons. *$P < 0.05$, **$P < 0.01$, ***$P < 0.001$.

Table 2. Clinical characteristics of HCC patients with NAFLD, HBV, or hepatic hemangioma.

Characteristics	Mean ± S.D/no (%)		
	NAFLD-related HCC ($n = 7$)	HBV-related HCC ($n = 12$)	Hepatic hemangioma ($n = 4$)
Sex, male	5 (71.4)	9 (56.3)	3 (75)
Age, year	53.9 ± 8.5	52 ± 14.5	41 ± 7
Body mass index, kg/m^2	29.6 ± 2.7	23 ± 2.9	25.1 ± 3.1
Waist-Hip ratio	0.9 ± 0.1	0.8 ± 0.1	0.8 ± 0.1
ALT, U/L	73.1 ± 42.6	47.6 ± 15.4	37.2 ± 11.3
AST, U/L	73.7 ± 43.9	51.3 ± 11.9	39.1 ± 2.1
GGT, U/L	60.2 ± 13.2	36.2 ± 8.8	35.1 ± 4.1
ALB, g/L	37.8 ± 3.5	37.7 ± 4.6	39.9 ± 2.7
Triglycerides, mmol/L	2.3 ± 0.8	1.7 ± 0.3	1.9 ± 0.5
Total cholesterol, mmol/L	5.4 ± 0.7	4.9 ± 0.9	5.2 ± 0.8
HDL cholesterol, mmol/L	1.2 ± 0.6	1.1 ± 0.2	1.5 ± 0.5
Total/HDL cholesterol, mmol/L	5 ± 1.4	4.7 ± 0.7	3.8 ± 1.3
Glucose, mmol/L	5.7 ± 0.7	4.9 ± 0.5	5.2 ± 0.5

hepatic haemangioma after surgery. The tissues were digested into a single-cell suspension and seeded into a three-dimensional culture system, and organoids were successfully established in vitro (Fig. 6a). Whole-mount immunofluorescence staining showed that the majority of cells expressed E-cadherin (Fig. 6b). After two weeks of cultivation, there were no significant differences in the number and size of organoids among the different groups (Fig. 6c, d). Organoid culture medium was collected to stimulate LX2 cells in the presence of PA-OA (Fig. 6a). Intriguingly, hepatocyte organoid conditional medium from NAFLD specimens stimulated HSCs activation, as evidenced by the upregulation of HSC activation-related genes, including *α-SMA*, *TGFB1*, *TIMP1*, *COL1A1*, *COL2A1*, and *MMP2* (Fig. 6f). ELISA confirmed higher levels of VEGFA in the organoid medium from the NAFLD-fibrosis group than those in the other two groups (Fig. 6e). Importantly, in this co-culture system, a close linear correlation was detected between VEGFA and the active HSC-related genes under NAFLD conditions (Figs. 6g, S5b). Furthermore, the VEGFA antibody α-VEGFA was used to inactivate VEGFA in the organoid medium. Interestingly, this activation was blocked by α-VEGFA (Fig. 6f). Together, these data strongly suggest that hepatocyte-derived VEGFA activates HSCs in patients with NAFLD-HCC.

DISCUSSION

The molecular mechanisms underlying NAFLD progression remain unclear. The complex interplay between hepatocytes and liver nonparenchymal cells plays a decisive role in the pathogenesis of NAFLD-HCC. Our study revealed that hepatocytes produce VEGFA to activate HSCs and promote the NAFLD-HCC transition. This result provides key information to our understanding of hepatocyte and HSC communication during NAFLD development. This highlights the potential of precise targeting of individual hepatic cell types as a therapeutic strategy for NAFLD and liver fibrosis.

Hepatocytes are the predominant functional cell population in the liver and play pivotal roles in energy metabolism, detoxification, and protein synthesis. Maintaining healthy hepatocytes is an important strategy for the development of new hepatoprotective drugs. In addition, therapies for controlling Kupffer cell or HSC activation may partially prevent the development of cirrhosis because of reactivation of proper hepatic crosstalk. At present, many drugs with anti-inflammatory or antioxidant capabilities have shown promising results on fibrosis in a lab setting but limited outcomes in clinical trials, possibly due to unknown effects on cellular crosstalk. Therefore, it is necessary to reveal new mechanisms of intercellular interactions at each stage of progression.

Pathological angiogenesis contributes to NAFLD development and promotes inflammation, fibrosis, and HCC progression. Although VEGFA is a key regulator of angiogenesis, the complexity of VEGFA biology raises concerns, including the non-angiogenic roles of VEGFA in both health and disease [26, 27]. In a mouse model of liver fibrosis resolution, VEGFA promoted fibrogenesis, but was also required for hepatic tissue repair and fibrosis resolution [28]. In the current study, hepatocytes produced VEGFA to promote fibrosis and endothelial dysfunction during the progression of NAFLD-HCC. When hepatic steatosis occurred in WD/CCl_4-WT mice at 12 weeks, VEGFA increased in the hepatocytes and was mainly distributed in the portal or periportal areas (Fig. 1h). Abnormalities in lipid metabolism may induce an increase in VEGFA. Fibrosis has been demonstrated as a major risk factor for malignant transition in patients with NAFLD [2, 29], but it is not fully clear how steatotic hepatocytes undergo malignant transition during the fibrogenic process. In our experiments, VEGFA deficiency in hepatocytes did not affect steatosis (Fig. 2e–h). Interestingly, some positive 8OHdG and p53BP1 cells were observed in the WD/CCl_4 NAFLD-HCC mouse model, whereas their expression was diminished in *Vegfa*$^{\Delta hep}$ mice (Fig. 3g, h). Given the technical limitations, we were unsure of the occurrence of DNA damage in all or partial steatotic hepatocytes, although the damage from WD/CCl_4 is a stronger inducer of carcinogenesis. *Tgfb1* and *Timp1* were downregulated in WD/CCl_4-*Vegfa*$^{\Delta hep}$ mice, which has been shown to promote malignant transformation [30, 31]. At present, it remains unclear whether hepatocyte-derived VEGFA acts directly or indirectly on the steatotic hepatocytes to undergo malignant transition during NAFLD-HCC formation. WD/CCl_4 promotes continuous liver damage and compensatory proliferation, which are critical processes in hepatocarcinogenesis. Tsuchida et al. revealed that liver histology and transcriptomic analysis of this model have a higher similarity to that of human patients, including alteration of metabolic pathways, expansion of hepatic progenitor cells (HPCs) and the extent of ductular reaction [19]. Combined with fibrosis alleviation in WD/CCl_4-*Vegfa*$^{\Delta hep}$ mice, we speculated that hepatocyte-produced VEGFA influencing NAFLD-HCC progression may be closely correlated with fibrosis and hepatic progenitor cell expansion. Given that VEGFA is a profibrogenic factor [32], our research further confirmed hepatocyte-derived VEGFA as a bridge molecule linking steatosis and fibrosis during NAFLD progression.

HBV- and NAFLD-HCC are long-term global health problems. The overall sequence of HCC development includes hepatocyte damage, fibrosis/cirrhosis, and hypoxic tissue conditions. Hypoxia triggers the production of several mediators, such as hypoxia-inducible factor 1α, VEGFA, and TGF-β1, which are all involved in liver fibrosis, cirrhosis, and HCC [9]. Temporal trends suggest that HBV-HCC is declining, whereas cryptogenic- or NAFLD-related HCC is an emerging clinical entity. A paradigm shift in the approach to the screening, surveillance, and management of HCC may be required in view of the changing landscape of HCC epidemiology into an increasing non-viral aetiology. In our study, there was no statistical difference in VEGFA levels or fibrosis scores between HBV- and NAFLD-cirrhotic specimens (Fig. 5a–c). Considering the specificity of hepatocytes and enrichment of immune cells in the liver, we established organoids from patients with NAFLD or HBV to further explore the interplay between hepatocytes and HSCs (Fig. 6a). The conditioned medium from NAFLD-derived organoids stimulated HSC activation, which was blocked by the VEGFA antibody (Fig. 6f). These results indicate that an increase in VEGFA

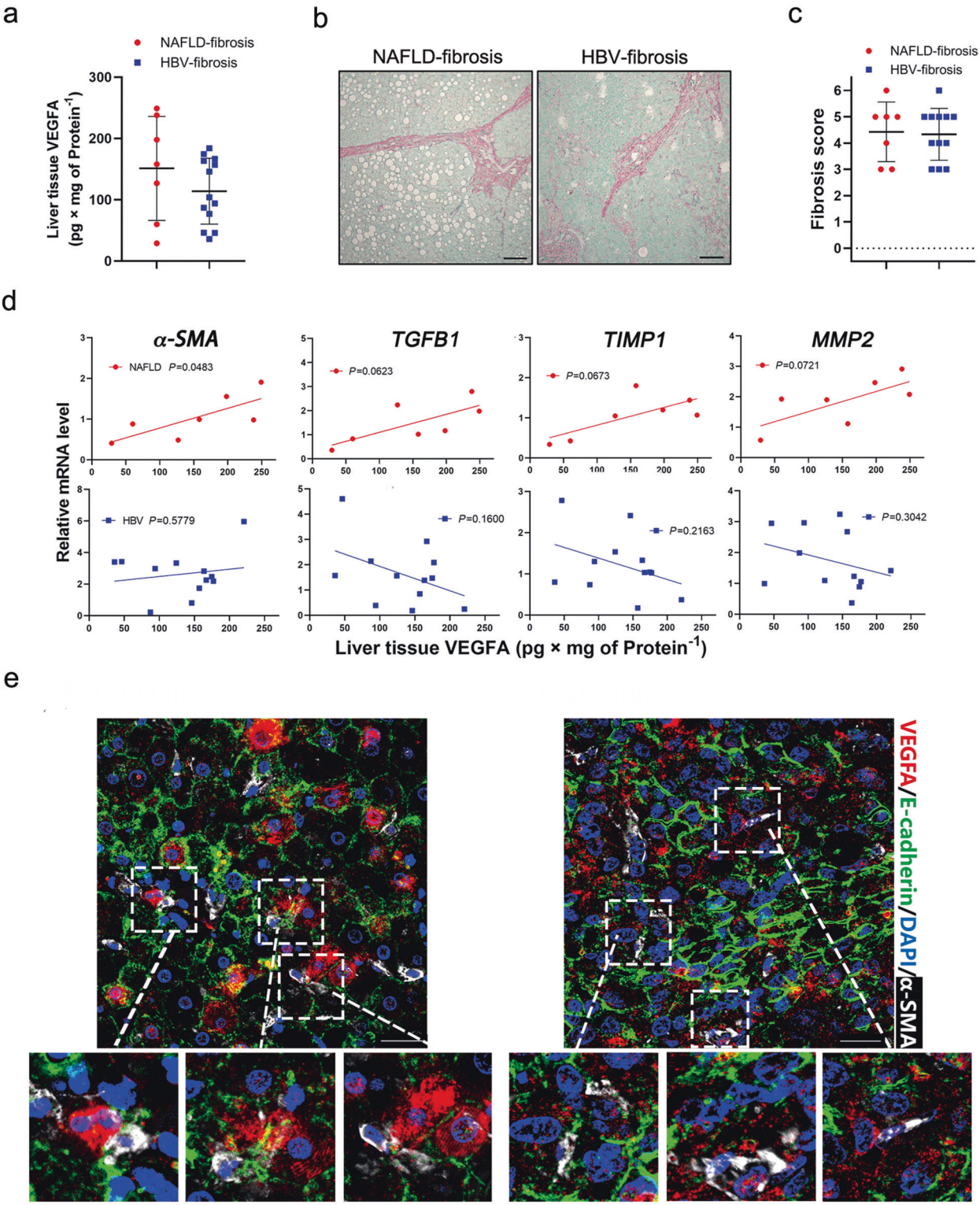

Fig. 5 The relationship between the expression of VEGFA and fibrotic genes in clinical NAFLD- or HBV-fibrosis specimens. a ELISA assay of VEGFA in clinical NAFLD- or HBV-fibrosis tissues (NAFLD, $n = 7$; HBV, $n = 12$). **b** Representative Sirius red staining in liver sections from (**a**). Scale bars, 150 μm. **c** Quantification of the fibrosis grade according to Ishak score of (**a**). **d** Correlation between the expression of VEGFA and fibrosis markers, *α-SMA*, *TGFB1*, *TIMP1*, and *MMP2* in (**a**). The Pearson correlation coefficient was calculated between two variables. **e** Representative immunofluorescence staining of VEGFA, E-cadherin, and α-SMA in (**a**). Scale bars, 25 μm.

in hepatocytes is the main stimulating factor for HSC activation in patients with NAFLD. Although the mechanism of NAFLD-induced VEGFA in hepatocytes is unclear, our data provide a clue for disentangling the pathogenies of HBV- and NAFLD-related HCC. The lack of correlation between VEGFA expression and HSC activation observed in HBV groups can be explained by other pathways responsible for HSCs activation, such as the Hedgehog/YAP or TGF-β/Notch pathways [33, 34]. Thus, appropriate targets

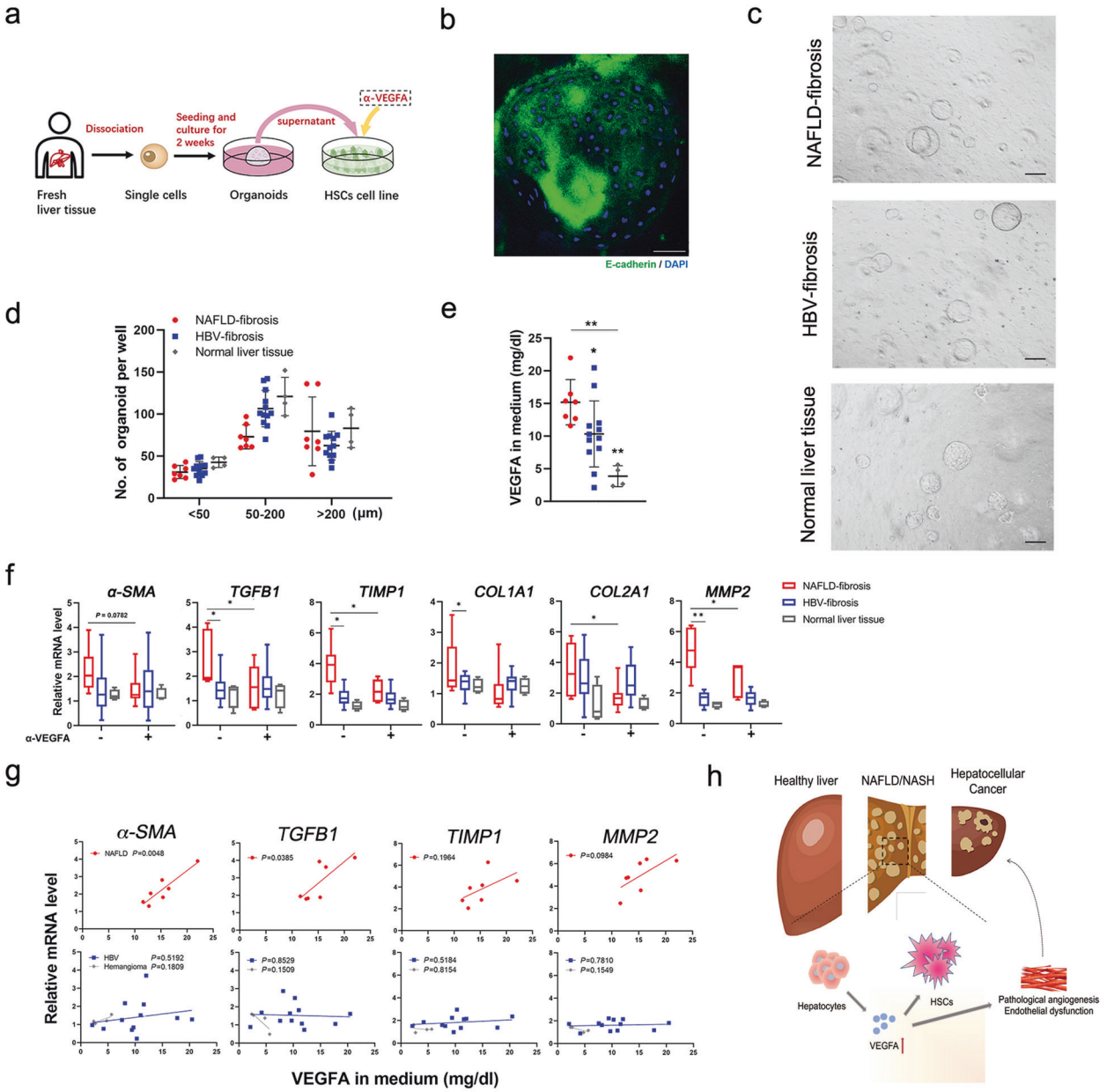

Fig. 6 Stimulation of LX2 cells with conditioned mediums from NAFLD patients-derived hepatocyte organoids. a Scheme representing experimental outline of hepatocyte organoids construction and stimulation of LX2 cells with conditioned medium. **b** Representative immunofluorescence staining of E-cadherin in organoids. Scale bars, 25 μm. **c** Representative bright-field image of hepatic organoids from clinical NAFLD-, HBV-fibrosis, and normal (hemangioma) liver tissues. Scale bars, 200 μm. **d** After 2 weeks in culture, organoid growth was monitored and quantification of number and size as indicated. Organoid size was recorded by a Leica microscope (NAFLD, $n = 7$; HBV, $n = 12$; haemangioma, $n = 4$). **e** ELISA assay of VEGFA in the conditioned medium from the three organoid groups (**c**). **f** LX2 cells were incubated with the conditioned medium from the three groups (**c**) for 72 h, and the mRNA levels of the indicated fibrosis molecules were determined by q-PCR in the presence or absence of α-VEGFA (2 μg/mL). **g** Correlation analysis between VEGFA protein levels in the conditioned medium from (**c**) and the mRNA levels of HSCs activation markers, *α-SMA, TGFB1, TIMP1 and MMP2*, in LX2 cells. The Pearson correlation coefficient was calculated between two variables. **h** Schematic depicting hepatocytes-derived VEGFA promoted NAFLD-HCC transition via activating HSCs. One-way ANOVA followed by Tukey's test was used for multiple comparisons. $^{*}P < 0.05$, $^{**}P < 0.01$.

for precise anti-fibrosis treatment are required for patients with chronic liver disease of different aetiologies.

In summary, we provide evidence that hepatocytes produce VEGFA to activate neighboring HSCs and accelerate the NAFLD-HCC transition, despite unaltered hepatic steatosis (Fig. 6h). Our data expand the essentiality of investigating VEGFA intervention via a cell-type-specific therapeutic strategy at different stages which will benefit precision medicine development for NASH and fibrosis.

DATA AVAILABILITY

The data that supports the findings of this study could be available from the corresponding author upon reasonable request.

ACKNOWLEDGEMENTS

We gratefully acknowledge the kind giving of *Vegfa*$^{fl/fl}$ mouse from Genentech (S. San Francisco). This study was supported by National Natural Science Foundation of China (81972584, 81988101, 81902904, 81830054, 81872231, 82073411), Shanghai

Education Commission (201901070007E00065), Program of Shanghai Academic/Technology Research Leader (20XD1405000), the Clinical Research Plan of SHDC (SHDC2020CR2011A).

AUTHOR CONTRIBUTIONS

HYW, YC, HS, and MCW conceptualized and designed the study. HS, HY, YTW, HD, QYL, JF, DC, LNG, LC, YY, and YX conducted the experiment and acquired data. HS and HY did the statistical analysis and drafted the paper. YC and HY revised the paper. HYW and YC supervised the experiment and provided funding support. All authors read and approved the final paper.

ADDITIONAL INFORMATION

Supplementary information The online version contains supplementary material available at https://doi.org/10.1038/s41401-022-00907-5.

Competing interests: The authors declare no competing interests.

Ethics approval: The study has been approved by the Research Ethics Committee of Eastern Hepatobiliary Surgery Hospital, and the informed consent has been obtained. All animal experiments were performed in accordance with the guidelines of the Institutional Animal Care and Use Committee of Second Military Medical University (Shanghai, China).

REFERENCES

1. Friedman SL, Neuschwander-Tetri BA, Rinella M, Sanyal AJ. Mechanisms of NAFLD development and therapeutic strategies. Nat Med. 2018;24:908–22.
2. Adams LA, Lymp JF, St Sauver J, Sanderson SO, Lindor KD, Feldstein A, et al. The natural history of nonalcoholic fatty liver disease: a population-based cohort study. Gastroenterology. 2005;129:113–21.
3. Wang X, Zheng Z, Caviglia JM, Corey KE, Herfel TM, Cai B, et al. Hepatocyte TAZ/WWTR1 promotes inflammation and fibrosis in nonalcoholic steatohepatitis. Cell Metab. 2016;24:848–62.
4. Lefere S, Van de Velde F, Hoorens A, Raevens S, Van Campenhout S, Vandierendonck A, et al. Angiopoietin-2 promotes pathological angiogenesis and is a therapeutic target in murine nonalcoholic fatty liver disease. Hepatology. 2019;69:1087–104.
5. Day CP. From fat to inflammation. Gastroenterology. 2006;130:207–10.
6. Jou J, Choi SS, Diehl AM. Mechanisms of disease progression in nonalcoholic fatty liver disease. Semin Liver Dis. 2008;28:370–9.
7. Bertolani C, Marra F. The role of adipokines in liver fibrosis. Pathophysiology. 2008;15:91–101.
8. Apte RS, Chen DS, Ferrara N. VEGF in signaling and disease: beyond discovery and development. Cell. 2019;176:1248–64.
9. Bocca C, Novo E, Miglietta A, Parola M. Angiogenesis and fibrogenesis in chronic liver diseases. Cell Mol Gastroenterol Hepatol. 2015;1:477–88.
10. Corpechot C, Barbu V, Wendum D, Kinnman N, Rey C, Poupon R, et al. Hypoxia-induced VEGF and collagen I expressions are associated with angiogenesis and fibrogenesis in experimental cirrhosis. Hepatology. 2002;35:1010–21.
11. Miura K, Ohnishi H, Morimoto N, Minami S, Ishioka M, Watanabe S, et al. Ezetimibe suppresses development of liver tumors by inhibiting angiogenesis in mice fed a high-fat diet. Cancer Sci. 2019;110:771–83.
12. Beraza N, Marques JM, Martinez-Anso E, Iniguez M, Prieto J, Bustos M. Interplay among cardiotrophin-1, prostaglandins, and vascular endothelial growth factor in rat liver regeneration. Hepatology. 2005;41:460–9.
13. European Association for the Study of the Liver. Electronic address eee, European Association for the Study of the L. EASL Clinical Practice Guidelines: Management of hepatocellular carcinoma. J Hepatol. 2018;69:182–236.
14. Yilmaz Y, Yonal O, Kurt R, Alahdab YO, Ozdogan O, Celikel CA, et al. Circulating levels of vascular endothelial growth factor A and its soluble receptor in patients with biopsy-proven nonalcoholic fatty liver disease. Arch Med Res. 2011;42:38–43.
15. Coulon S, Francque S, Colle I, Verrijken A, Blomme B, Heindryckx F, et al. Evaluation of inflammatory and angiogenic factors in patients with non-alcoholic fatty liver disease. Cytokine. 2012;59:442–9.
16. Tarantino G, Conca P, Pasanisi F, Ariello M, Mastrolia M, Arena A, et al. Could inflammatory markers help diagnose nonalcoholic steatohepatitis? Eur J Gastroenterol Hepatol. 2009;21:504–11.
17. Wang B, Fu J, Yu T, Xu A, Qin W, Yang Z, et al. Contradictory effects of mitochondria- and non-mitochondria-targeted antioxidants on hepatocarcinogenesis by altering DNA repair in mice. Hepatology. 2018;67:623–35.
18. Broutier L, Andersson-Rolf A, Hindley CJ, Boj SF, Clevers H, Koo BK, et al. Culture and establishment of self-renewing human and mouse adult liver and pancreas 3D organoids and their genetic manipulation. Nat Protoc. 2016;11:1724–43.
19. Tsuchida T, Lee YA, Fujiwara N, Ybanez M, Allen B, Martins S, et al. A simple diet- and chemical-induced murine NASH model with rapid progression of steatohepatitis, fibrosis and liver cancer. J Hepatol. 2018;69:385–95.
20. Kornek M, Raskopf E, Guetgemann I, Ocker M, Gerceker S, Gonzalez-Carmona MA, et al. Combination of systemic thioacetamide (TAA) injections and ethanol feeding accelerates hepatic fibrosis in C3H/He mice and is associated with intrahepatic up regulation of MMP-2, VEGF and ICAM-1. J Hepatol. 2006;45:370–6.
21. Francque SM, van der Graaff D, Kwanten WJ. Non-alcoholic fatty liver disease and cardiovascular risk: Pathophysiological mechanisms and implications. J Hepatol. 2016;65:425–43.
22. Ma C, Kesarwala AH, Eggert T, Medina-Echeverz J, Kleiner DE, Jin P, et al. NAFLD causes selective $CD4^+$ T lymphocyte loss and promotes hepatocarcinogenesis. Nature. 2016;531:253–7.
23. Mederacke I, Hsu CC, Troeger JS, Huebener P, Mu X, Dapito DH, et al. Fate tracing reveals hepatic stellate cells as dominant contributors to liver fibrosis independent of its aetiology. Nat Commun. 2013;4:2823.
24. McGlynn KA, Petrick JL, El-Serag HB. Epidemiology of hepatocellular carcinoma. Hepatology. 2021;73:4–13.
25. Su HJ, Kao JH, Tseng TC, Yang HC, Su TH, Chen PJ, et al. Pathologic findings of patients with nonalcoholic fatty liver disease and the impact of concurrent hepatitis B virus infection in Taiwan. J Formos Med Assoc. 2020;119:1476–82.
26. Barratt SL, Flower VA, Pauling JD, Millar AB. VEGF (vascular endothelial growth factor) and fibrotic lung disease. Int J Mol Sci. 2018;19:1269.
27. Ntellas P, Mavroeidis L, Gkoura S, Gazouli I, Amylidi AL, Papadaki A, et al. Old player-new tricks: non angiogenic effects of the VEGF/VEGFR pathway in cancer. Cancers. 2020;12:3145.
28. Yang L, Kwon J, Popov Y, Gajdos GB, Ordog T, Brekken RA, et al. Vascular endothelial growth factor promotes fibrosis resolution and repair in mice. Gastroenterology. 2014;146:1339–50.e1.
29. Powell EE, Wong VW, Rinella M. Non-alcoholic fatty liver disease. Lancet. 2021;397:2212–24.
30. Caballero-Diaz D, Bertran E, Penuelas-Haro I, Moreno-Caceres J, Malfettone A, Lopez-Luque J, et al. Clathrin switches transforming growth factor-beta role to pro-tumorigenic in liver cancer. J Hepatol. 2020;72:125–34.
31. Ordonez R, Carbajo-Pescador S, Prieto-Dominguez N, Garcia-Palomo A, Gonzalez-Gallego J, Mauriz JL. Inhibition of matrix metalloproteinase-9 and nuclear factor kappa B contribute to melatonin prevention of motility and invasiveness in HepG2 liver cancer cells. J Pineal Res. 2014;56:20–30.
32. Foglia B, Sutti S, Pedicini D, Cannito S, Bocca C, Maggiora M, et al. Oncostatin M, a profibrogenic mediator overexpressed in non-alcoholic fatty liver disease, stimulates migration of hepatic myofibroblasts. Cells. 2019;9:28.
33. Du K, Hyun J, Premont RT, Choi SS, Michelotti GA, Swiderska-Syn M, et al. Hedgehog-YAP signaling pathway regulates glutaminolysis to control activation of hepatic stellate cells. Gastroenterology. 2018;154:1465–79.e13.
34. Zhang K, Han X, Zhang Z, Zheng L, Hu Z, Yao Q, et al. The liver-enriched lnc-LFAR1 promotes liver fibrosis by activating TGFbeta and Notch pathways. Nat Commun. 2017;8:144.